Journal of Ceramic Processing Research. Vol. 10, No. 3, pp. 391~400 (2009)

J O U R N A L O F
Ceramic Processing Research

Estimation of residual stress by instrumented indentation: A review

Jae-il Jang*
Division of Materials Science and Engineering, Hanyang University, Seoul 133-791, Korea

Since residual stresses that are often generated in many components and devices by thermal mismatch or thermal/mechanical processing can strongly affect their mechanical performance and reliability, there has been considerable scientific and engineering interest in non-destructively determining the residual stresses in ceramics, glasses and metals. In this regard, recently much effort has been made to develop new methods of residual stress measurement using an instrumented indentation technique (especially nanoindentation). In the present paper, the recently-developed methods are critically reviewed and related issues are discussed in terms of advantages and shortcomings of each method, in order to provide some insight for future research in the field.

Key words: Residual stress, Instrumented Indentation, Nanoindentation

Introduction

In many engineering components and devices made of various materials (including ceramics, metals, and glasses), residual stresses can be introduced by thermal mismatch or mechanical/thermal processing during their manufacturing, welding/joining, and sintering operations [1-4]. For example, residual stresses can be generated in a thin film system from the thermal expansion mismatch between the film and substrate during cooling in the deposition process. Similarly, in engineering alloys reinforced with hard ceramic particles, residual stresses can be produced during cooling from the processing temperature, by the thermal expansion mismatch between the ceramic particles and the metal matrix. Also, in a welded metal joint, significant residual stresses are caused by the welding thermal cycle that generates inhomogeneous heating and cooling in the regions near the heat source.

It is well known that residual stresses can strongly affect the mechanical performance (such as the static and fatigue strengths, fracture toughness, corrosion-/wear-resistance) and thus the reliability and lifetime of components and devices in a negative or positive way. For instance, if a structural component is under an externally applied tensile stress, compressive residual stresses enhance the resistance to crack propagation, whereas tensile residual stresses deteriorate the resistance. For semiconductor devices, residual stresses can lead to a sharp decrease in their service life, but under the appropriate internal (or residual) stresses, the mobility of charge carriers and thus the speed of the device can be significantly increased [5]. Therefore, from an engineering viewpoint, to properly measure the residual stresses can be very important in order to achieve a reliable engineering design of components and devices.

A variety of methods for the measurement of residual stresses are currently available [1-4]. The conventional methods can be divided into two groups: mechanical stress-relaxation methods and physical-parameter analysis methods. Mechanical stress-relaxation methods, including a strain-gauge method for a bulk material (e.g., hole-drilling and saw-cutting technique) and a curvature measurement method for a film/coating system (e.g., layer-removal technique), can generally be used to directly and destructively evaluate residual stress without any reference sample. However, their destructive nature limits the wide application of these techniques in industry. Whereas, physical-parameter analysis methods (e.g., analysis of X-ray diffraction, ultrasonic wave, magnetic Barkhausen noise, neutron diffraction, and Raman spectra) can measure residual stresses indirectly and nondestructively, and the former three methods among them have been partially used in industrial fields. However, it is always difficult to separate intrinsic microstructural effects on the physical parameters from the effects of a residual stress, and hence the methods require the preparation of stress-free reference sample for comparison purposes. Additionally, the physical methods cannot be directly applied to amorphous/glass materials (such as a large-scale glass display panel and a shot-peened bulk metallic glass) that do not have a long-range ordered atomic structures.

One more technique to be added into the list of residual stress measurement methods is instrumented indentation (especially nanoindentation) that has rapidly emerged in the past two decades as a powerful tool for exploring mechanical behavior of a small volume. The instrumented indentation has made it possible to measure a variety of mechanical properties (e.g., hardness [6, 7], Young's modulus

*Corresponding author:
Tel : +82-2-2220-0402
Fax: +82-2-2220-0389
E-mail: jijang@hanyang.ac.kr

[6, 7], yield strength [8, 9], work-hardening exponent [10, 11], creep stress exponent [12, 13], fracture toughness [14, 15]) and small-scale mechanical behavior (e.g., indentation size effect [16, 17], pressure-induced phase transformation of semiconductors [18, 19], inhomogeneous deformation of amorphous alloys [20, 21]) only by analyzing the indentation load-displacement (*P-h*) curve without the need to observe a hardness impression using a microscopy. Recently many studies have been undertaken to develop new ways to measure residual stress using instrumented indentation, because this non-destructive/mechanical technique may overcome the limitations of conventional methods including both the destructive/mechanical and nondestructive/physical methods. Although a number of reviews on instrumented indentation and nanoindentation are available in literature [5, 22-31], to the best of my knowledge, no review is fully devoted to the application of the technique to residual stress measurement. The present paper reviews the fundamentals and recent advances in the ways to estimate residual stresses through instrumented indentation test.

Early Studies Using a Conventional Hardness Test

The investigations for measuring residual stress using instrumented indentation was originally motivated by earlier hardness studies in which the change in hardness by the applied uniaxial or biaxial stresses was observed through conventional Rockwell or Vickers hardness tests. In 1932, Kokubo [32] performed experiments on various metals (including steels, brass, Al, Cu, etc.) to show the effect of strain on hardness measurements. In the study, he applied a bending stress to cause 0.3% strain on the outer surface of the specimen and performed Vickers hardness tests at a peak load of 5 kg_f on the surface of the specimen under the strained state. Then, he reported that applied tensile stresses made the material appear 5~12% softer while compressive stresses caused only a 0~3% increase in apparent hardness.

Based on Kokubo's work [32], Sines and Carlson [33] performed Rockwell hardness tests on a high carbon steel bar under an applied 4-point bending stress, and suggested a way of 'hardness measurements for determination of residual stresses' (which is the title of their paper). A representative result in their work is shown in Fig. 1 (which was reproduced in [34]). It is clear that, if the applied stress is tensile, the material appears softer as the applied stress is increased although the change in hardness is small (less than 10%). An applied compressive stress seems to make the material appear a little harder, but the change in hardness is almost negligible (less than 1%). Thus, the influence of stress was greater for specimens loaded in tension than those loaded in compression.

In 1950, Pomey *et al.* [35] suggested a method of measuring residual stress based on the observation that surface residual stress affected the yield strength which was obtained when a spherical indentation was made on

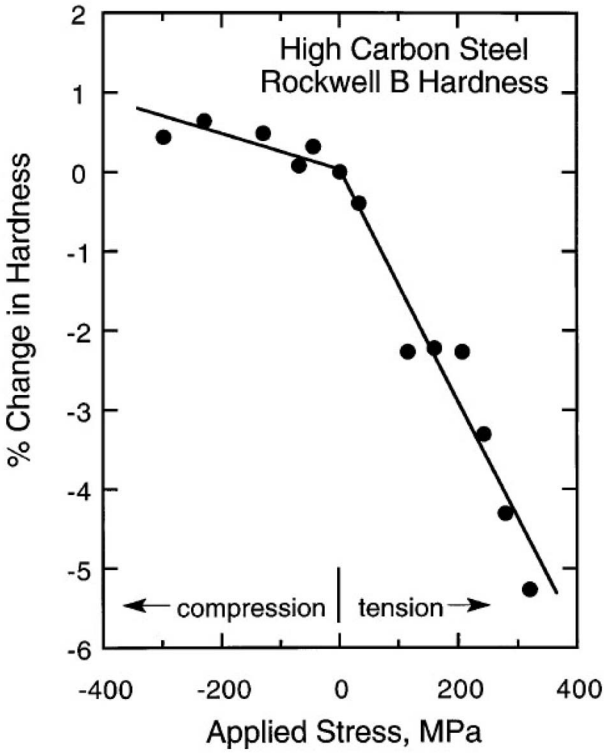

Fig. 1. Change in Rockwell B hardness produced by uniaxial stresses in a high carbon steel bent bar (reproduced in [34] using the data of [33]).

the smooth surface of the test specimen. While a hard spherical indenter with a diameter of 0.4~1.5 mm was pressed with increasing load, the electric resistance of the contact point was recorded. A sudden fall in resistance occurred when the material beneath the indenter became plastic. The corresponding load gave the surface stresses of the specimen. In 1973, Underwood [36] estimated the residual stress by examining the shape of the pile-up occurring at the edge of the contact circle. Deviations in shape provided some information about the level and sign of residual stress within the specimen.

One of the most popular methods used to estimate residual stresses in brittle ceramics and glasses using a conventional hardness test is indentation cracking test (typically performed for estimating indentation fracture toughness). Some researchers have examined the critical load of crack initiation to determine the magnitude and direction of surface residual stress in brittle materials [37]. Chaudhri and Phillips [38], and Chandrasekar and Chaudhri [39] reported that the residual stress can be determined by:

$$\sigma_R = \frac{\psi(P_{c(R)} - P_c)}{1.6c^2} \quad (1)$$

where c is the length from the center of hardness impression to the crack tip, $P_{c(R)}$ and P_c are the loads that produce cracks of the same c in glass with and without a residual stress, respectively, and ψ is a constant dependent on

the indenter geometry; for a Vickers indenter,

$$\psi = \frac{1}{\pi^{3/2} tan(68^{\circ})} \quad . \tag{2}$$

In some investigations performing indentation cracking tests, the size of radial cracks generated with a sharp Vickers indenter in brittle solids has been used as a means of determining the residual stresses. Zeng and Rowcliffe [40, 41] carried out indentation cracking tests on glass, and proposed that one can estimate residual stresses if a comparison is made of the equation for the indentation fracture toughness of the unstressed material;

$$K_C = \chi\left(\frac{P}{c^{3/2}}\right) \tag{3}$$

and that for the toughness of the material under a residual stress, given by:

$$K_C = \chi\left(\frac{P}{c_R^{3/2}}\right) \pm \sigma_R c_R^{0.5} \eta \quad . \tag{4}$$

Here, K_C is the indentation fracture toughness, χ is a constant (depending on the indenter geometry, Young's modulus, and hardness), η is the crack geometry factor, c and c_R are the length from the center of the impression to the crack tip for the unstressed and stressed material respectively. In Eq. (4), the positive sign is for a tensile stress and the negative one is for a compressive stress. Noting that the same χ and P are involved in both expressions, the residual stress can be solved by combining Eqs. (3) and (4):

$$\sigma_R = \pm K_C \left[\frac{1-(c/c_R)^{3/2}}{\eta\sqrt{c_R}}\right] \quad . \tag{5}$$

A similar approach was made for a thin-film system by Zhang *et al.* [42], and Kese and Rowcliffe [43] demonstrated that Eq. (5) holds valid for nanoindentation fracture toughness tests using a cube-corner indenter having a centerline-to-face angle of 35.3° that is much sharper than a typical Berkovich indenter (with the angle of 65.3°).

Initial Observations Using Instrumented Indentation

Since its commercialization in the middle of the 1980s, instrumented indentation technique (especially nanoindentation) has proven to be a powerful tool for measuring small-scale mechanical properties of materials. Unlike conventional hardness tests measuring hardness by imaging a hardness impression, instrumented indentation provides the mechanical properties purely by analyzing the curve of indentation load, P, vs. the penetration displacement, h, both of which are recorded during entire loading and unloading sequences. Fig. 2 exhibits a typical load-displacement (P-h) curve of an indentation made with a sharp indenter. From the curve, the indentation hardness H (which is equal to the mean contact pressure, p_m) can be determined by:

$$H = p_m = \frac{P_{\max}}{A_C} \tag{6}$$

where A_C is the projected contact area that may be a geometrical function of the contact depth, h_C. For example, $A_C = 24.5 h_C^2$ for an ideal Berkovich tip. According to the most popular method proposed by Oliver and Pharr [7], the contact depth can be given by:

$$h_C = h_{max} - \omega \frac{P_{max}}{S} \tag{7}$$

where ω is a geometric parameter that is 0.72 for a cone, 0.75 for a Berkovich tip and rounded tip, and 1 for a flat punch, and S is the stiffness that can be measured as the initial slope of the unloading curve (see Fig. 2).

Perhaps the first reported attempt to measure a residual stress by analyzing the nanoindentation P-h curve is that of LaFontaine *et al.* [44] who examined the nanoindentation hardness (obtained by P-h curve analysis) of thin aluminum films thermally processed to produce a biaxial tensile stress as high as 380 MPa. X-ray diffraction analysis revealed that during aging (for ~100 h) at room temperature the biaxial stress relaxed by ~50% and the nanoindentation hardness increased by ~200%. Based on the observed relationship between the residual stress and nanoindentation hardness, they suggested a simple way to extract the residual stress (σ_R) from nanoindentation experiments, which can be given as:

$$\sigma_{Y,app} = \sigma_Y + b\sigma_R \tag{8}$$

and

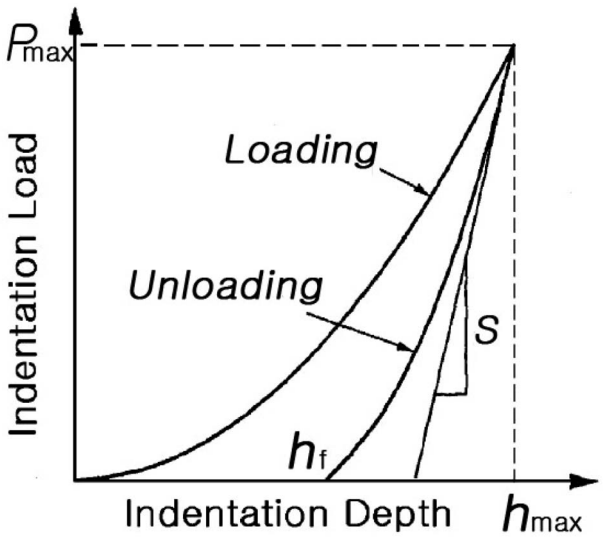

Fig. 2. Typical example of a load-displacement curve recorded during instrumented indentation [7,22].

$$\sigma_R = \frac{\delta H}{bC} \tag{9}$$

Here $\sigma_{Y,app}$ and σ_Y are the uniaxial yield strength of a material with and without residual stress respectively, b is a proportionality constant, δH is the change in nanoindentation hardness due to the presence of a residual stress, and C is the constraint factor that can be empirically determined by [45-46]:

$$H = p_m = C\sigma \tag{10}$$

where σ is the yield strength or the flow stress at an representative strain underneath the indenter. Although the residual stresses estimated by nanoindentation tests are in a good agreement with those measured by X-ray diffraction, no clue to the physical meaning of the proportionality constant (b) and how to determine it was provided in the paper.

Nanoindentation research on the issue of residual stress measurement accelerated in the middle of 1990s with the systematic analysis of the residual stress effects on the indentation behavior by both experiments and simulations reported in two companion papers by Tsui *et al.* [34] and Bolshakov *et al.* [47]. In the first paper by Tsui *et al.* [34], a series of nanoindentation experiments were performed on Al 8009 alloy samples under either uniaxially or biaxially applied stresses. When the hardness was measured according to Oliver-Pharr method [7], a change in hardness with the applied stress (which might be replaced by the residual stress for a real system) was clearly observed, i.e., the hardness increased with the applied compressive stress, and decreased with the applied tensile stress, which is in a good agreement with the results in earlier studies using conventional hardness tests [32, 33]. However, their successive, careful examination of real indentation contact areas using optical micrographs at high magnification (taken with an oil immersion lens) revealed that the hardness change with the applied stress was not a fact, but rather an experimental artifact caused by the influence of stress on the geometry of material pile-up around the hardness impression. Fig. 3 compares the contact area A_C measured optically and that predicted from a P-h curve analysis [34]. It is obvious that, for the examined Al 8009 alloy, the real contact area (measured optically) is essentially independent of the applied stress while the contact area predicted from the curve shows a strong dependence on the stress. According to Eq. (6), this means that the optically-measured hardness might be almost independent of applied stress while the hardness by the Oliver-Pharr method is strongly dependent on the stress. From these results, Tsui *et al.* [34] concluded that, for the Al 8009 sample under a compressive stress, due to the pile-up developed around the edges of a hardness impression, the hardness by the Oliver-Pharr method was overestimated by an amount up to as large as 15%. Curiously, however, the stress-independence of real hardness is in direct contrast to results obtained from conventional hardness tests [32, 33].

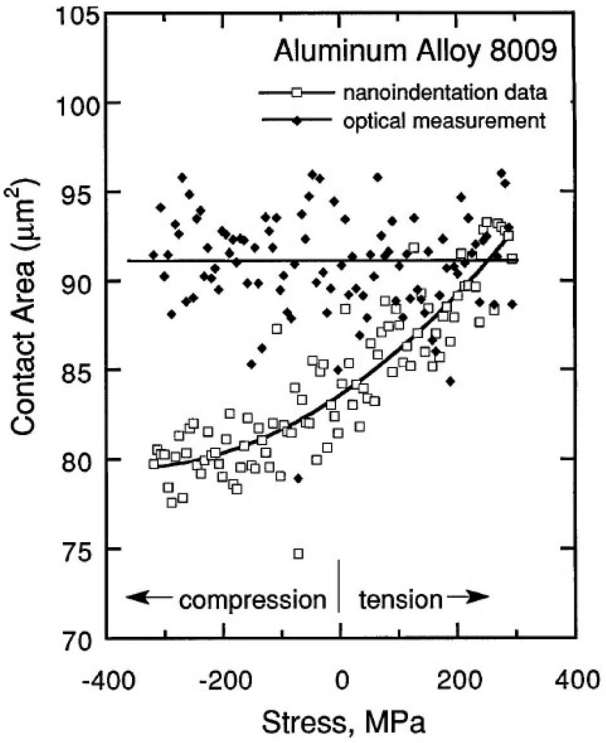

Fig. 3. A comparison of optically measured contact areas with those predicted from analysis of nanoindentation P-h curves [34].

In a follow-up study by Bolshakov *et al.* [47], a series of finite element simulations of elastic-plastic indentations in the Al 8009 alloy were performed to establish how the indentation pile-up is influence by an applied (or residual) stress. As a result, it was confirmed that the failure to properly account for the pile-up in the Oliver-Pharr method gives rise to an artificial dependence of the measured hardness and elastic modulus on the applied stress. Also, they suggested an important feature as schematically shown in Fig. 4; the shape of the loading curve (and the unloading curve that is not shown here) deviates from the ideal shape of the unstressed sample, even if the deviation is often too small to be accurately measured during nanoindentation experiments.

Although these two studies [34, 47] did not provide a detailed procedure for determining residual stress using nanoindentation (or instrumented indentation), they gave an important insight that motivated much following research on the issue: while real hardness may not be influenced by residual stress, the nanoindentation hardness estimated by the curve analysis (according to the Oliver-Pharr method) can be seriously affected by the stress. Thus, one may conceivably estimate the residual stress by analyzing the deviation in the shape of the indentation curve from the ideal shape. Following the above studies, Zagrebelny and Carter [48] experimentally proved that the curve shift due to a residual stress also occurs in a silicate-glass system as shown in Fig. 5.

It is interesting to note that, independently of the above studies, a similar observation of a P-h curve shift was

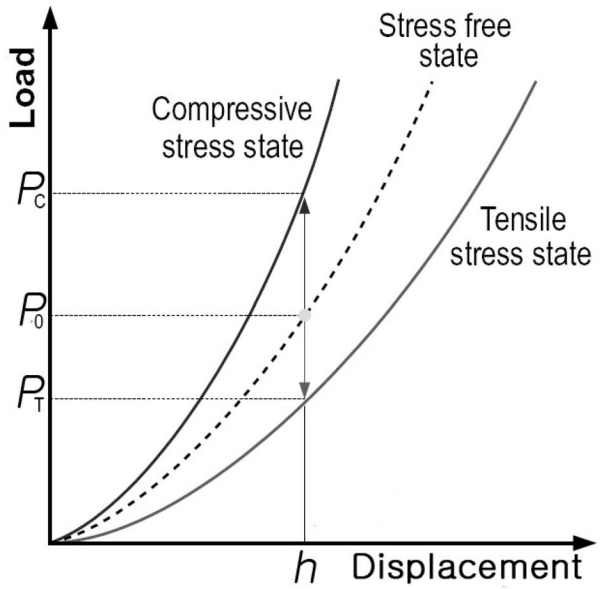

Fig. 4. Shift of the indentation loading curve with change in stress state.

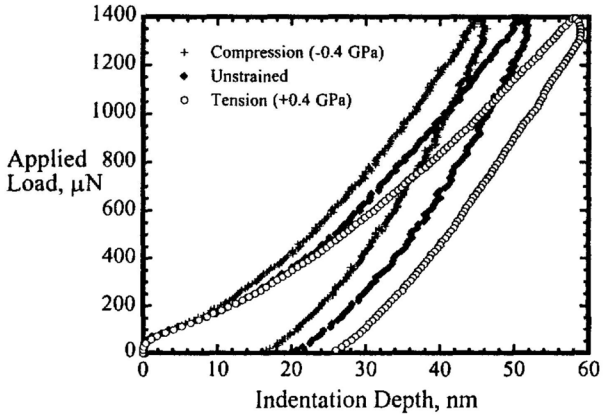

Fig. 5. An example of a nanoindentation P-h curve shift due to a residual stress [48].

reported in Japan, though it has not been well recognized. Ishihara and Oku [49] performed micro-indentation on the surface of a specimen under uniaxial tensile loading. It was found that the *P-h* curve of the specimen under a tensile residual strain of 0.2% exhibited a higher peak-load displacement than that of a stress-free specimen.

Models for Instrumented Sharp Indentation

Model by Suresh and Giannakopoulos

The work of Tsui *et al.* [34] and Bolshakov *et al.* [47] demonstrated that the shape of the indentation curve and thus the 'apparent' hardness are indeed affected by a residual stress in a manner that might be useful in characterizing the stress. This led Suresh and Giannakopoulos [50] to propose a simple methodology for estimating a residual stress through instrumented indentation with a sharp indenter. Their model is on the basis of two assumptions; first, the elastic equi-biaxial residual stress at the surface is uniform over the depth of influence of the indenter; second, an equi-biaxial residual stress state at the indented surface would be equivalent to a hydrostatic stress plus a uniaxial stress component that can induce a differential indentation force.

Then, they considered the influence of a residual stress on the indentation curve shape and thus estimated the residual stress by taking the variation in the contact area into account. In the case of a tensile stress, they suggested as an equation:

$$\frac{A_{app,free}}{A_{app,R}} = \left(1 - \frac{\sigma_R}{H}\right) . \tag{11}$$

where $A_{app,R}$ is the apparent contact area of the sample under a residual stress and $A_{app,free}$ is the apparent contact area of the stress-free sample. In the case of a compressive residual stress:

$$\frac{A_{app,free}}{A_{app,R}} = \left(1 + \frac{\sigma_R \sin\alpha}{H}\right). \tag{12}$$

Here α is the inclination of a sharp indenter to the surface, i.e., $\alpha = 22^\circ$ for a four-sided pyramidal Vickers indenter, 24.7° for a three-sided pyramidal Berkovich indenter, and 19.7° for an equivalent conical indenter. Note that the difference between Eq. (11) and (12) agrees well with the nonlinear trend from compression to tension, as observed earlier [32-34]. However, because the stress influence on the contact area is relatively small in nanoindentation experiments (Tsui *et al.* [34] found the maximum change in hardness to be no more than 10%), this method may be practical only when the residual stress is very high (near the yield stress) and only in those materials in which material pile-up is pronounced. This may make it difficult to use the method for general practical applications.

Model by Carlsson and Larsson

Carlsson and Larsson [51, 52] analyzed sharp indentation behavior to explore how an equi-biaxial residual stress and strain fields can be determined from the contact area A and the indentation hardness H. In the first paper reporting the numerical simulation results [51], they recognized that residual strain fields can be accurately correlated with the hardness value while residual stresses are related to the size of the contact area. That is, a residual compressive stress enhanced the pile-up and thus increased the real contact area, while a residual tension stress reduced the real contact area.

As a result, they found that, for a sharp indentation, a new indentation parameter c^2 that is the ratio of A (the real contact area of a sample showing sink-in or pile-up) to A_{nom} (the nominal contact area directly calculated from the indentation depth h_{max} without consideration of sink-in or pile-up along the contact boundary) can be estimated by:

$$\frac{A}{A_{nom}} = c^2(\varepsilon_R, \sigma_R) = c^2(\varepsilon_R, \sigma_R = 0) - 0.32 \ln\left(1 + \frac{\sigma_R}{\sigma}\right). \quad (13)$$

In this equation, σ is the yield strength (σ_Y) for an elastic-fully plastic material and the flow stress at a given strain under a residual stress [$\sigma(\varepsilon_R)$] for a strain-hardening material. As $c^2(\varepsilon_R, \sigma_R = 0)$ are close to unity in most cases of interest (i.e., a significant pile-up or sink-in cannot be developed without a residual stress), Eq. (13) for an elastic-fully plastic material can be simplified by applying the first-order approximation (i.e., σ_R/σ_Y is very small):

$$c^2(\varepsilon_R, \sigma_R) \approx 1 - 0.32 \frac{\sigma_R}{\sigma_Y}. \quad (14)$$

If $H \sim 3\sigma_Y$ is assumed [45], the right term in Eq. (14) is very close to that of Eq. (11) proposed by Suresh and Giannakopoulos [50]. However, unlike Suresh and Giannakopoulos's approach, Carlsson and Larsson did not set the normal stress component to zero, and instead, they suggested using the apparent yield stress at the corresponding representative strain [$\sigma(\varepsilon_R)$]. In the second companion paper [52], Carlsson and Larsson experimentally verified the applicability of Eq. (13), although they did not provide a solution for a general residual stress state.

Model by Lee and colleagues

Lee and colleagues [53-55] modified the idea of Suresh and Giannakopoulos [50] by interpreting the effect of the equi-biaxial residual stress as the normal component in the resulting deviatoric part of the stress tensor according to the following equation:

Equi-biaxial stress Mean stress Deviator stress

$$\begin{bmatrix} \sigma_R & 0 & 0 \\ 0 & \sigma_R & 0 \\ 0 & 0 & 0 \end{bmatrix} = \begin{bmatrix} \frac{2}{3}\sigma_R & 0 & 0 \\ 0 & \frac{2}{3}\sigma_R & 0 \\ 0 & 0 & \frac{2}{3}\sigma_R \end{bmatrix} + \begin{bmatrix} \frac{1}{3}\sigma_R & 0 & 0 \\ 0 & \frac{1}{3}\sigma_R & 0 \\ 0 & 0 & -\frac{2}{3}\sigma_R \end{bmatrix}. \quad (15)$$

The stress component parallel to the indentation axis in the deviator stress term ($\sigma_{zz} = -2\sigma_R/3$) directly affects the indentation-induced plastic deformation. Thus, they found that the contribution of an equi-biaxial residual stress on the normal indentation force P_R can be defined from the selected deviator stress component in Eq. (15):

$$P_R = \frac{2}{3}\sigma_R A_C \quad (16)$$

In this equation, P_R is the contribution to the indentation force caused by the residual stress and can be experimentally measured as the difference in force P between stressed and unstressed samples at a given displacement (see Fig. 4).

In subsequent investigations [56, 57], they extended and validated their model towards a general residual stress state by introducing the stress ratio (κ) as the ratio of the minor in-plane residual stress component σ_R^y to the major in-plane residual stress component σ_R^x, i.e. $\sigma_R^y = \kappa\sigma_R^x$. Inserting the stress ratio k into the previous equation, they obtained an expression:

$$P_R = \frac{-(1+\kappa)}{3}\sigma_R^x A_C. \quad (17)$$

It was found that the experiments were in good agreement with this relation. Perhaps this model has the widest practical application in the literature. This may be because instrumented micro-indentation experiment at high loads (instead of nanoindentation) was mostly performed in their work, and hence the relatively small curve shift in nanoindentation could be enlarged.

It is noteworthy that there are limitations in the above three models for sharp indentations; that is, the models of Suresh and Giannakopoulos [50] and Carlsson and Larsson [51, 52] are restricted to an equi-biaxial residual stress; Lee *et al.*'s [56, 57] model provides a way to consider the biaxial residual stress, but cannot describe the well-known nonlinearity from tension to compression [33, 34]. Very recently, Huber and Heerens [58] pointed out these limitations and suggested by spherical indentation simulations that the limitations might be overcome if the ratio of the contact pressure for the residual stress state to the contact pressure for the stress-free state is analyzed based on the von Mises J_2-flow criterion.

Models for Instrumented Spherical Indentation

Because the residual stress effect on a sharp indentation is generally small as mentioned above, Taljat and Pharr [59] considered whether residual stresses could be better measured with a spherical indenter. Finite element simulations on spherical indentations revealed a significant effect of an equi-biaxial stress on the indentation load-displacement (*P-h*) behavior, but only in the 'elastic-plastic transition' regime.

To examine whether or not the effect is experimentally measurable, Swadener *et al.* [60] performed spherical nanoindentation experiments on polished disks of several aluminum alloys that could be stressed to prescribed levels of equi-biaxial tension and compression (see Fig. 6). They found that tensile stresses shift the nanoindentation *P-h* curves to appreciably larger depths by enhancing plasticity, while compressive stresses have the opposite effect. Based on these observations, Swadener *et al.* [60] developed two different methods for measuring the residual stress using spherical indenters, as follows.

The first method is based on the fact that the measured depth at which yielding occurs is affected by the stress in a manner that can be analyzed by Hertzian contact mechanics. For a spherical indentation in the purely elastic deformation regime (i.e., for Hertzian contact), the mean

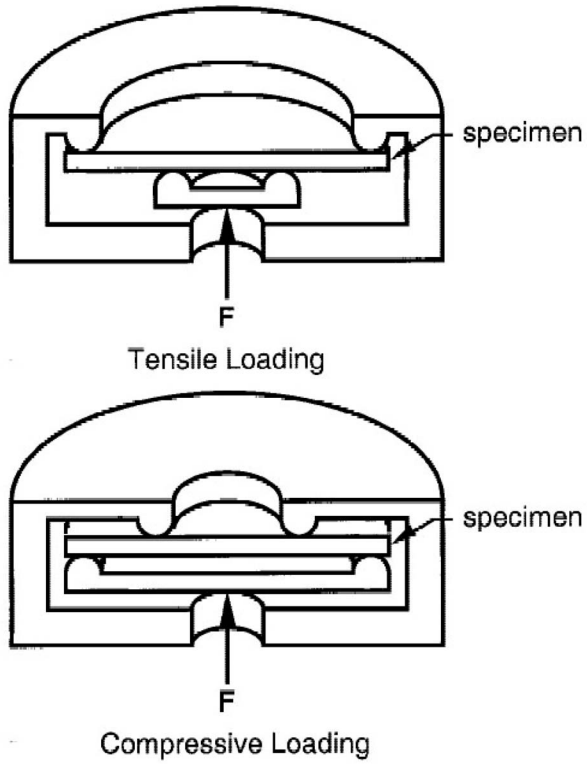

Fig. 6. Schematic illustration of axi-symmetric bending apparatus [60].

contact pressure p_m under the indenter during elastic deformation can be related to the contact radius of the spherical indenter, a, by:

$$P_m = \frac{P_{\max}}{\pi a^2} = \frac{4E_r a}{3\pi R} \tag{18}$$

where R is the radius of the indenter, E_r is the reduced elastic modulus determined from the Young's modulus E and Poisson's ratio n of the specimen and the indenter. The contact radius a can be determined by consideration of the spherical indenter geometry:

$$a = (2Rh_C - h_C^2)^{0.5} \tag{19}$$

where the contact depth h_C for a spherical indentation can be given as:

$$h_C = \frac{1}{2}(h_{max} + h_f) \tag{20}$$

In Eq. (20), $h_{\max}$ can be directly measured from a P-h curve, but the final depth of the contact impression after unloading h_f can be better obtained by curve fitting (second-order polynomial) the upper 90% of the unloading curve.

To determine the mean contact pressure p_m at the onset of yielding, it is necessary to plot the measured elastic recovery parameter ($h_f/h_{\max}$) against the non-dimensional plasticity index, $E_r a/\sigma_Y R$ [46], at various indentation loads. Since $h_f/h_{\max} = 0$ represents purely elastic deformation, the plasticity index at $h_f/h_{\max} = 0$ signifies the onset of

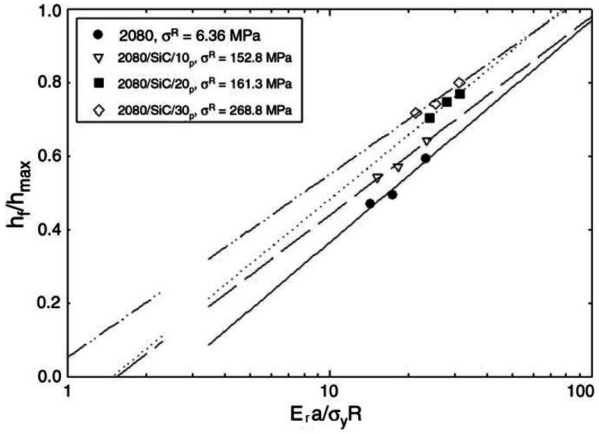

Fig. 7. An example to show the variation in the elastic recovery parameter with the non-dimensional plasticity index [61].

yielding and is used to determine the contact radius at the yielding point a_0. Both numerical and experimental analysis have shown that a nearly linear relationship exists between $h_f/h_{\max}$ and $\log(E_r a/\sigma_Y R)$ over a wide range of elastic-plastic transition. In Fig. 7, an example of the linear relation experimentally obtained by Olivas *et al.* [61] is shown. Thus, by extrapolating the discrete data set of $\log(E_r a/\sigma_Y R)$ to $h_f/h_{\max} = 0$, one can obtain the desired a_0.

At the onset of yielding, Johnson [46] showed using either the Tresca or the von Mises yield criterion that the constraint factor C [in Eq. (10)] is 1.07 (often ~1.1). When an equi-biaxial residual stress σ_R is present in the material, Taljat and Pharr [59] have shown by finite element analysis (FEA) that the onset of yielding is determined by the superposition of the biaxial and Hertzian stresses. As long as yielding initiates below the surface along the axis of symmetry, Eq. (10) can be rewritten as:

$$P_m = 1.07(\sigma_Y - \sigma_R) \tag{21}$$

where p_m is positive and σ_R is positive (or negative) for tension (or compression). Combining Eq. (18) and (21):

$$\frac{\sigma_R}{\sigma_Y} = 1 - \frac{3.72}{3\pi}\left(\frac{E_r a_0}{\sigma_Y R}\right) \tag{22}$$

Therefore, if σ_Y is given, the residual stress σ_R can be determined by the measurement of $(E_r a_0/\sigma_Y R)$ by the extrapolation method mentioned above. However, the difficulties in application of this method are that the σ_Y of the material should be known independently and that data has to be extrapolated outside the range of experimental accessibility. Also, this method may need a very large indenter radius in the experiments.

Swadener *et al.*'s [60] second method is based on their interesting empirical observation of the relationship between the mean contact pressure p_m and the non-dimensional plasticity index ($E_r a/\sigma_Y R$). Since E_r and σ_Y are material constants, their observation can be simplified

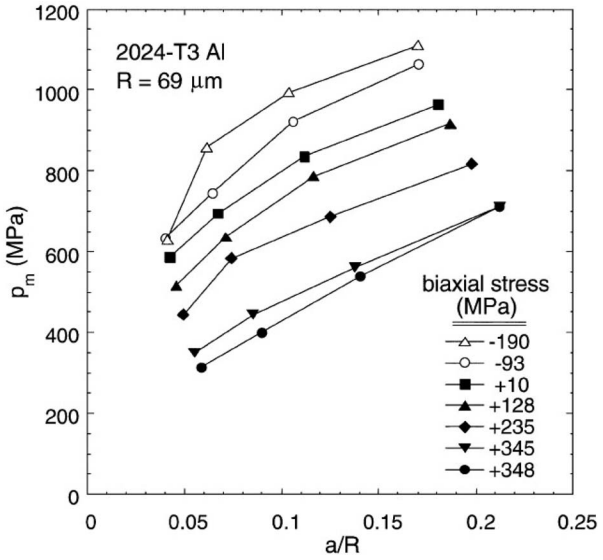

Fig. 8. Dependence of the mean pressure on m the normalized contact radius, a/R, for indentation of 2024-T3 aluminum. Biaxial stress influences are manifested as vertical shifts of the curves [62].

as shown in Fig. 8 [62]. In this figure, data for 2024-T3 aluminum are plotted as the mean contact pressure, p_m, vs. the normalized contact radius, a/R. At a given equi-biaxial stress, the pressure steadily increases with a/R, as would be expected since increasing a/R corresponds to driving the indenter in to greater depths. However, the feature of interest is that the plots are vertically shifted by an amount very close to the relative level of the applied biaxial stress. This observation suggests that for a specimen with a residual stress, Eq. (10) should be rewritten as:

$$p_m + \sigma_R = C\sigma_f \tag{23}$$

If the variation in ($C\sigma_f$) with ($E_r a/\sigma_Y R$), or simply (a/R), can be established by experiments in a reference material in a known stress state, then σ_R can be determined from measurements of the indentation contact pressure p_m. From a careful analysis of their experimental data, Swadener *et al.* [60] concluded that the above two methods can be used to measure residual stresses to within 10-20%. Recently, Olivas *et al.* [61] reported that the surface residual stress in SiC particle-reinforced Al matrix composites can be successfully estimated by using the first method explained above.

Other Recent Studies Using Numerical Simulations

In addition to the theoretical models reviewed above, some research has applied numerical simulations and fitted these data to establish the influence of a residual stress on instrumented indentation behavior [63-69].

Chen and co-workers [63] performed finite element simulations of sharp indentation behavior systematically to analyze the effects of both the ratio of the in-plane residual stress to the yield strength, σ_R/σ_Y, and the reciprocal yield strain, E/σ_Y, on the hardness H, the stiffness S (see Fig. 2), and the work of plastic deformation $W_{pl} = \int_0^{h_{max}} P dh$. It was found that the normalized hardness is essentially independent of residual stress when $E/\sigma_Y > 300$, but when $E/\sigma_Y < 300$, a tensile residual stress enhances the plastic flow and decreases the hardness. The normalized stiffness was significantly increased (or decreased) by the tensile (or compressive) residual stress, but only when $E/\sigma_Y < 30$. For $E/\sigma_Y > 30$, the normalized stiffness is invariant (~1.1). The normalized plastic work appears to have a wide spread for both σ_R/σ_Y and E/σ_Y. Based on the results, Chen and co-workers proposed an algorithm of reverse analysis to extract σ_R, σ_Y, and E from the known single P-h curve (i.e., information about hardness, stiffness, and the plastic work), which may make it possible to estimate the residual stress without the requirement of a stress-free reference sample. Since their first study [63] was restricted to an equi-biaxial stress state and elastic-fully plastic solids, Chen and co-workers have attempted to extend their approach to a uni-axial stress state [64] and to strain-hardening materials [65].

In contrast to other simulation studies, Xu and Li [66-67] have mainly focused on the equi-biaxial residual stress effects on the 'unloading' behavior of nanoindentation. Fig. 9 shows the variation in the shape of the unloading curve for an elastic-fully plastic material having $E/\sigma_Y = 100$ [66]. In the figure, a compressive residual stress increases the elastic recovery ratio of h_e (= 1 – h_f) to h_{max} while a tensile residual stress reduces the ratio. From extensive finite element simulations, it was revealed that there is a nearly linear relationship between the h_e/h_{max} and σ_R/σ_Y, and its slope is only dependent on the E/σ_Y ratio but independent of the strain-hardening behavior. Oppositely, the slope of the linear relation between the contact area ratio A/A_{nom} (where A is the real contact area and A_{nom} is the nominal contact area calculated from the indentation depth according to the indenter geometry; this ratio was defined as c^2 by Carlsson and Larsson [51,52]) and σ_R/σ_Y is independent of the E/σ_Y ratio, but dependent on the A/A_{nom} ratio. Based on these above relations, Xu and Li [67] proposed a coupled nanoindentation-bending method for determining the residual stress in a mechanically polished fused quartz beam. Although they emphasized that this method does not need to use any stress-free reference sample, the need for a bending jig and relatively complex specimen geometry may restrict its practical application.

Concluding Remarks

In this paper, research on the residual stress measurements using instrumented indentation has been reviewed. Now, there have been many studies in which successful applications of the technique are reported. Although applying instrumented indentation for that purpose has clear advantages due to the nature of the technique as a simple non-destructive/mechanical test, there are some issues still remaining unresolved.

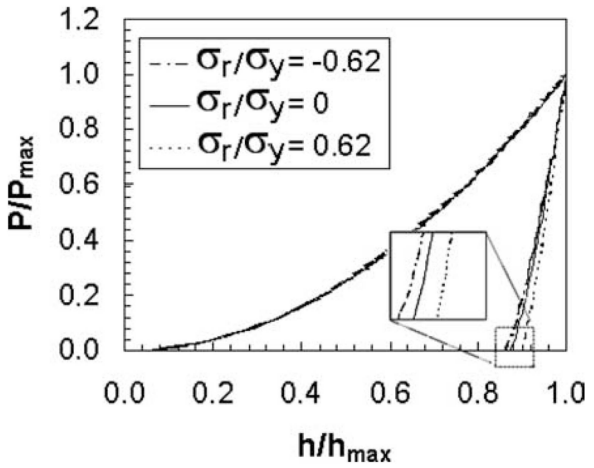

Fig. 9. The influence of the residual stress on the unloading curve of indentation [66].

First of all, many methods reviewed here require the need for a stress-free reference sample. The reference sample should have a microstructure almost identical to the test specimen. In reality, this may be difficult to achieve in many cases, especially in a material having a significant microstructural gradient. Lepienski *et al.* [62] pointed out that a stress-free reference sample for a thin film system is very hard to be obtained. This is because only annealing can relax the residual stresses of a thin film, but it can also change the microstructure and thus the intrinsic mechanical properties.

Another practically important issue is that the current indentation methods cannot be applied to a material showing a strong dependency of the residual stress on its direction while the indenters basically give an average response of the surface residual stress. Note that residual stress states determined by current instrumented indentation techniques are mostly restricted to equi-biaxial or uni-axial stress. Although some models [56] provide general residual stress solutions, the stress ratio k should be known independently. Some efforts have been given to obtain information about the stress-directionality by measuring the direction-dependency of pile-up height [70], this way necessitates the careful observation of the indentation morphology. Very recently some attempts have been made using an asymmetric Knoop indenter [71], but the method has not been fully established yet.

Finally, as Lepienski *et al.* [62] proposed, how to properly consider the influence of both the surface roughness and the substrate on the residual stresses in a thin film system is also an issue to be solved in future.

Acknowledgement

This research was supported partly by the Korea Institute of Energy Technology Evaluation and Planning (KETEP) grant funded by MKE (Grant # 2008-P-EP-HM-E-04-0000) and partly by the Korea Science and Engineering Foundation (KOSEF) grant funded by MEST (Grant # R01-2008-000-20778-0).

References

1. I.C. Noyan and J.B. Cohen, Residual Stress; Measurement by Diffraction and Interpretation, Springer-Verlag, New York, (1987).
2. V. Hauk, Structural and Residual Stress Analysis by Non-destructive Methods, Elsevier, New York, (1997).
3. J. Lu and M.R. James (ed.), Handbook of Measurement of Residual Stresses, Fairmount Press, Liburn, GA, (1996).
4. K. Masubuchi, Analysis of Welded Structures: Residual Stresses, Distortion, and their Consequences, Pergamon Press, New York, (1980).
5. Y.I. Golovin, Physics of the Solid State 50 (2008) 2205-2236.
6. M.F. Doerner and W.D. Nix, J. Mater. Res. 1 (1986) 601-609.
7. W.C. Oliver and G.M. Pharr, J. Mater. Res. 7 (1992) 1564-1583.
8. J.S. Field and M.V. Swain, J. Mater. Res. 10 (1995) 101-112.
9. M.V. Swain, Mater. Sci. Eng. A 253 (1998) 160-166.
10. M. Dao, N. Chollacoop, K.J. Van Vliet, T.A. Venkatesh and S. Suresh, Acta Mater. 49 (2001) 3899-3918.
11. J.-I. Jang, Y. Choi, Y.-H. Lee, J.-S. Lee, D. Kwon, M. Gao and R. Kania, Int. J. Fracture 131 (2005) 15-34.
12. B.N. Lucas and W.C. Oliver, Metall. Mater. Trans. A 30 (1999) 601-610.
13. H. Li and A.H.W. Ngan, J. Mater. Res. 19 (2004) 513-522.
14. R.F. Cook and G.M. Pharr, J. Am. Ceram. Soc. 73 (1990) 787-817.
15. J.-I. Jang and G.M. Pharr, Acta Mater. 56 (2008) 4458-4469.
16. W.D. Nix and H. Gao, J. Mech. Phys. Solids 46 (1998) 411-425.
17. J.G. Swadener, E.P. George and G.M. Pharr, J. Mech. Phys. Solids 50 (2002) 681-694.
18. V. Domnich and Y. Gogotsi, Appl. Phys. Lett. 76 (2000) 2214-2216.
19. J.-I. Jang, M.J. Lance, S. Wen, T.Y. Tsui and G.M. Pharr, Acta Mater. 53 (2005) 1759-1770.
20. C.A. Schuh and T.G. Nieh, J. Mater. Res. 19 (2004) 46-57.
21. J.-I. Jang, B.-G. Yoo and J.-Y. Kim, Appl. Phys. Lett. 90 (2007) Art. No. 211906.
22. W.C. Oliver and G.M. Pharr, J. Mater. Res. 19(2004) 3-20.
23. Y.-T. Cheng and C.-M. Cheng, Mater. Sci. Eng. R 44 (2004) 91-149.
24. G.M. Pharr, Mater. Sci. Eng. A 253 (1998) 151-159.
25. A.C. Fischer-Cripps, Vacuum 58 (2000) 569-585.
26. X. Li and B. Bhushan, Mater. Characterization 48 (2002) 11-36.
27. B. Bhushan and X. Li, Int. Mater. Reviews 48 (2003) 125-164.
28. N.K. Mukhopadhyay and P. Paufler, Int. Mater. Reviews 51 (2006) 209-245
29. C.A. Schuh, Mater. Today 9(5) (2006) 32-40.
30. A. Gouldstone, N. Chollacoop, M. Dao, J. Li, A.M. Minor and Y.-L. Shen, Acta Mater. 55 (2007) 4015-4039.
31. A.C. Fischer-Cripps, Nanoindentation, Springer-Verlag, New York, 2002.
32. S. Kokubo, "Change in hardness of a plate by bending," Science Reports of the Tohoku Imperial University (Series 1) 21 (1932) 256-267.
33. G. Sines and R. Carlson, "Hardness measurement for determination of residual stresses," ASTM Bulletin 180 (1952, Feb.) 35-37.
34. T.Y. Tsui, W.C. Oliver and G.M. Pharr, J. Mater. Res. 11 (1996) 752-759.
35. J. Pomey, F. Goutel and L. Abel, Publications scientifiques et Techniques du Ministere de l'Air No. 263 (1950).
36. J.H. Underwood, Experimental Mechanics 30 (1973) 373-380.
37. S.G. Roberts, C.W. Lawrence, Y. Bisrat and P.D. Warren, J.

Am. Ceram. Soc. 82 (1999) 1809-1816.
38. M.M. Chaudhri and M.A. Philipps, Phil. Mag. A 62 (1990) 1-27.
39. S. Chandrasekar and M.M. Chauhari, Phil. Mag. A 67 (1993) 1187-1218.
40. K. Zeng and D.J. Rowcliffe, J. Am. Ceram. Soc. 77 (1994) 524-530.
41. K. Zeng and D.J. Rowcliffe, Acta Metall. Mater. 43 (1995) 1935-1943.
42. T.-Y. Zhang, L.-Q. Chen and R. Fu, Acta Mater. 47 (1999) 3869-3878.
43. K. Kese and D.J. Rowcliffe, J. Am. Ceram. Soc. 86 (2003) 811-816.
44. W.R. LaFontaine, C.A. Paszkiet, M.A. Korhonen and C.-Y. Li, J. Mater. Res. 6 (1991) 2084-2090.
45. D. Tabor, Hardness of metals, Clarendon press, Oxford, UK, 1951.
46. K.L. Johnson, Contact mechanics, Cambridge Univ. Press, Cambridge, UK, 1985.
47. A. Bolshakov, W.C. Oliver and G.M. Pharr, J. Mater. Res. 11 (1996) 760-768.
48. A.V. Zagrebelny and C.B. Carter, Scripta Mater. 37 (1997) 1869-1875.
49. M. Ishihara and T. Oku, Trans. JSME A 62 (1996) 2305-2309.
50. S. Suresh and A.E. Giannakopoulos, Acta Mater. 46 (1998) 5755-5767.
51. S. Carlsson and P.-L. Larsson, Acta Mater. 49 (2001) 2179-2191.
52. S. Carlsson and P.-L. Larsson, Acta Mater. 49 (2001) 2193-2203.
53. Y.-H. Lee and D. Kwon, Scripta Mater. 49 (2003) 459-465.
54. J.-I. Jang, D. Son, Y.-H. Lee, Y. Choi and D. Kwon, Scripta Mater. 48 (2003) 743-748.
55. Y.-H. Lee, D. Kwon and J.-I. Jang, Int. J. Modern Phys. B 17 (2003) 1141-1146.
56. Y.-H. Lee and D. Kwon, Acta Mater. 52 (2004) 1555-1563.
57. Y. Lee, J.-Y. Kim, J.-S. Lee, K.-H. Kim, J.Y. Koo and D. Kwon, Phil. Mag. 86 (2006) 5497-5504.
58. N. Huber and J. Heerens, Acta Mater. 56 (2008) 6205-6213.
59. B. Taljat and G.M. Pharr, Mat. Res. Sco. Symp. Proc. 594 (2000) 519-524.
60. J.G. Swadener, B. Taljat and G.M. Pharr, J. Mater. Res. 16 (2001) 2091-2102.
61. E.R. Olivas, J.G. Swadener and Y.-L. Shen, Scripta Mater. 54 (2006) 263-268.
62. C.M. Lepienski, G.M. Pharr, Y.J. Park, T.R. Watkins, A. Misra and X. Zhang, Thin Solids Films 447-448 (2004) 251-257.
63. X. Chen, J. Yan and A.M. Karlsson, Mater. Sci. Eng. A 416 (2006) 139-149.
64. M. Zhao, X. Chen, J. Yan and A.M. Karlsson, Acta Mater. 54 (2006) 2823-2832.
65. J. Yan, A.M. Karlsson and X. Chen, Int. J. Solids. Struc. 44 (2007) 3720-3737.
66. Z.-H. Xu and X. Li, Acta Mater. 53 (2005) 1913-1919.
67. Z.-H. Xu and X. Li, Phil. Mag. 86 (2006) 2835-2846.
68. L.Z. Liu, Y.W. Bao and Y.C. Zhou, J. Mater. Res. 21 (2006) 1680-1686.
69. T.E. Buchheit and R. Tandon, J. Mater. Res. 22 (2007) 2875-2887.
70. Y.-H. Lee, K. Takashima, Y. Higo and D. Kwon, Scripta Mater. 51 (2004) 887-891.
71. J.-H. Han, J.-S. Lee, Y.-H. Lee, M.-J. Choi, G. Lee, K.-H. Kim and D. Kwon, Key Eng. Mater. 345-346 (2007) 1125-1128.